INTERFACE SCIENCE

Interfacial interaction of solid cobalt with liquid Pb-free Sn–Bi–In–Zn–Sb soldering alloys

V. I. Dybkov · V. G. Khoruzha · V. R. Sidorko ·
K. A. Meleshevich · A. V. Samelyuk · D. C. Berry ·
K. Barmak

Abstract Dissolution kinetics of cobalt in liquid 87.5%Sn–7.5%Bi–3%In–1%Zn–1%Sb and 80%Sn–15% Bi–3%In–1%Zn–1%Sb soldering alloys and phase formation at the cobalt–solder interface have been investigated in the temperature range of 250–450 °C. The temperature dependence of the cobalt solubility in soldering alloys was found to obey a relation of the Arrhenius type $c_s = 4.06 \times 10^2 \exp(-46300/RT)$ mass% for the former alloy and $c_s = 5.46 \times 10^2 \exp(-49200/RT)$ mass% for the latter, where R is in J mol^{-1} K^{-1} and T in K. For tin, the appropriate equation is $c_s = 4.08 \times 10^2 \exp(-45200/RT)$ mass%. The dissolution rate constants are rather close for these soldering alloys and vary in the range $(1–9) \times 10^{-5}$ m s^{-1} at disc rotational speeds of 6.45–82.4 rad s^{-1}. For both alloys, the $CoSn_3$ intermetallic layer is formed at the interface of cobalt and the saturated or undersaturated solder melt at 250 °C and dipping times up to 1800 s, whereas the $CoSn_2$ intermetallic layer occurs at higher temperatures of 300–450 °C. Formation of an additional intermetallic layer (around 1.5 μm thick) of the $CoSn$ compound was only observed at 450 °C and a dipping time of 1800 s. A simple mathematical equation is proposed to evaluate the intermetallic-layer thickness in the case of undersaturated melts. The tensile strength of the cobalt-to-solder joints is 95–107 MPa, with the relative elongation being 2.0–2.6%.

V. I. Dybkov (✉) · V. G. Khoruzha · V. R. Sidorko ·
K. A. Meleshevich · A. V. Samelyuk
Department of Physical Chemistry of Inorganic Materials,
Institute for Problems of Materials Science, 03180 Kyiv, Ukraine
e-mail: vdybkov@ukr.net; vdybkov@ipms.kiev.ua

D. C. Berry · K. Barmak
Department of Materials Science and Engineering,
Carnegie Mellon University, Pittsburgh, PA 15213, USA

Introduction

In view of worldwide legislation (for example, European Union's Waste Electrical and Electronic Equipment Directive 2002/95/EC) for the gradual reduction and further removal of some heavy metals (lead, mercury, cadmium, etc.) from all new equipments and products put on the market, there is an urgent need for the development of lead (Pb)-free solders and research on metal–solder joint behavior under various performance conditions. Since Pb falls into the range of toxic metals, conventional Sn–Pb solders are being replaced mainly with Sn-based soldering alloys containing additions of other low-melting point metals. It is not surprising, therefore, that Pb-free solders are receiving significant attention in scientific and technical communities. For example, at the TMS 2007 Annual Meeting, the programme included a one-day workshop on Pb-free solders and 11 technical sessions on Pb-free solders and phase transformations. As evidenced from the literature [1–32], most frequently employed additives to tin to develop new Pb-free solders are Ag, Au, Cu, Bi, In, Zn, and Sb.

During soldering of solid metals or alloys, two physicochemical processes, namely, dissolution of the solid in the liquid phase and formation of intermetallic-compound layers at their interface take place simultaneously after wetting the solid surface with a molten solder. Although crucial in choosing optimum conditions of the soldering procedure, available data on the kinetics of the two processes for most Pb-free solders are still fragmentary and scarce.

The occurrence of intermetallic-compound layers that are too thick considerably deteriorates the mechanical strength of the transition zone between dissimilar materials. Usually, the intermetallics occur both at the phase interface between a

solid metal or alloy being soldered and a Sn-based soldering alloy in the form of a brittle continuous layer and in its vicinity in the melt material as the aggregation of relatively coarse grains. The former occurs in the course of a chemical reaction, while the latter forms either during cooling of the melt, or, in some cases, as a result of destroying the layer under the influence of the liquid phase. Note that at constant temperature and pressure no intermetallic compound can exist in the bulk of the solder melt, even if saturated in the course of dissolution of the solid phase. Its crystallization only starts when the temperature drops (pressure is usually constant), so that the melt becomes supersaturated with atoms of a dissolving substance.

It should be emphasized that the complete absence of intermetallic-compound layers between dissimilar metals or alloys does not necessarily provide evidence for their reliable joining. In reality, the absence of intermetallics may just be due to the lack of contact between joined materials because of presence of oxide films, surface contaminations, etc. at phase interfaces, that excludes any chemical reaction. Clearly, if no reaction occurs, no metallurgical bonding of the materials is possible. Therefore, in practice, the concept of a permissible intermetallic-layer thickness is essential. This is the maximal thickness of the intermetallic layer which still does not affect noticeably the mechanical strength of the joint. At the same time, the presence of such a layer provides evidence of the occurrence of chemical interaction between joined materials. For different pairs of metals and alloys, the permissible intermetallic-layer thickness may vary in the range 0.5–5 μm. Its precise value for each particular couple can only be found experimentally. Once it is determined, the parameters of the joining process may be evaluated on the basis of the layer thickness–time dependence (the so-called growth law of the layer).

Conventionally, the intermetallic-layer growth kinetics are treated with the use of parabolic equations following from Fick's laws on the assumption of quasi-stationary distribution of the concentration of any component within growing layers [33–36]. However, if the solubility of a solid metal in a liquid soldering alloy is not zero, as is practically always the case, then the growth rate constant found experimentally proves time dependent. Actually, it means that those equations do not provide an adequate description of the kinetics of the intermetallic-layer growth process for systems with a noticeable solubility in the liquid state, and the so-called growth law thus established is only valid under strict experimental or technological conditions, remaining unspecified in most cases.

To overcome this drawback, in the framework of a physico-chemical analysis of the reaction–diffusion process in solid–liquid systems, a general three-term mathematical equation describing the intermetallic-layer growth kinetics under conditions of its simultaneous dissolution in a molten soldering alloy was derived [37]. From this equation, it follows that the intermetallic-layer thickness can in many cases be reduced to a permissible level solely by increasing the dissolution rate of a solid in a liquid, without employing any additional technological operations.

In this work, data on the interfacial interaction of solid cobalt with liquid 87.5%Sn–7.5%Bi–3%In–1%Zn–1%Sb and 80%Sn–15%Bi–3%In–1%Zn–1%Sb soldering alloys at 250–450 °C are reported. According to binary phase diagrams [38], all four chosen additives (Bi, In, Zn, and Sb) lower the melting-point temperature of tin. To avoid undesirable phase transformations, In, Zn, and Sb were taken in the amounts not exceeding their solid-state solubility limits in tin. These elements are known to improve service characteristics of Sn-based solders [39].

Since the main component of Pb-free Sn–Bi–In–Zn–Sb solders is tin, intermetallic layers based on the Co–Sn compounds may be expected to form at the cobalt–solder interface in the course of soldering. Four intermetallic compounds Co_3Sn_2, $CoSn$, $CoSn_2$, and $CoSn_3$ are known to exist in the Co–Sn binary system [40–44]. Although diffusional considerations [45] predict the simultaneous parabolic growth for the layers of all intermetallics available on an appropriate binary phase diagram, this does not always seem to be the case. More often, layer formation is sequential, with at most two compound layers growing simultaneously under conditions of diffusion control (see, for example, [37]).

With the above background in mind, the aim of this work is threefold:

(i)   to determine the parameters (solubility, dissolution-rate constant, and diffusion coefficient) characterizing dissolution kinetics of solid cobalt in molten Pb-free 87.5%Sn–7.5%Bi–3%In–1%Zn–1%Sb and 80%Sn–15%Bi–3%In–1%Zn–1%Sb soldering alloys at 250–450 °C;

(ii) to establish which of the intermetallic compounds are formed as separate layers between solid cobalt and liquid solders; and

(iii) to visualize the effect of dissolution on the growth rate of the intermetallic-compound layer and its morphology.

Experimental procedure

Materials and specimens

Electrolytic-grade cobalt (99.98% Co, major impurities: 0.005% Ni, 0.005% C, 0.003% Fe, 0.001% Al, and 0.001% Zn) plates; tin (99.915% Sn, 0.025% Pb, 0.015% Sb, 0.010%

Bi, 0.010% As, 0.010% S, and 0.010% Cu); bismuth (99.999% Bi, 3×10^{-4}% Pb, $<3 \times 10^{-4}$% Ni, $<3 \times 10^{-4}$% Cr, and 1×10^{-4}% Sn); indium (99.999% In, 5×10^{-4}% Ti, 1×10^{-4}% Pb, 1×10^{-4}% Sn, and 1×10^{-4}% Zn); and antimony (99.91% Sb, 0.03% Pb, 0.02% Sn, 0.02% As, 0.01% Fe, and 0.01% S) slabs and zinc granules (99.95% Zn, 0.02% Pb, 0.01% Cd, and 0.01% Fe) were employed for the investigation. All contents are given in mass percent unless otherwise stated.

Pieces of cobalt were re-melted in an electric-arc furnace to obtain 12- to 13-mm-diameter rods. Cylindrical specimens were machined from these rods. Sn-based soldering alloys of required composition were prepared by melting their components Sn, Bi, In, Zn, and Sb together under a flux in a specially designed device and subsequent casting from 700 °C into a massive copper mold to ensure rapid cooling. Pieces of these alloys were then used as a melt material.

Experimental methods

The process of dissolution of cobalt in liquid Pb-free Sn-based soldering alloys and that of growth of intermetallic layers under conditions of their simultaneous dissolution in the liquid phase have been studied by the rotating disc technique using a rapid-quenching device [37]. Schematic diagram illustrating the dissolution process of cobalt in liquid soldering alloys is shown in Fig. 1. Briefly, the experimental procedure was as follows.

To heat the materials under investigation to the required temperature and to maintain it, the electric-resistance furnace is employed. The specimen of solid cobalt is connected, by means of a graphite protective tube, with the shaft being rotated at a pre-determined speed in the 6.45–82.4 rad s^{-1} range by an electric motor. The shaft is free to

Fig. 1 Schematic diagram to illustrate the process of dissolution of cobalt in a liquid soldering alloy in the case where no chemical compound layer is formed at their interface. Not to scale. In fact, the thickness, δ, of the diffusion boundary layer is negligibly small in comparison with the height of the column of the liquid phase

move in the vertical direction and can be fixed in the required position by a stopper. The temperature is measured with the help of a thermocouple. A flux is used both to pre-heat the solid specimen to the experimental temperature and to protect the melt from oxidation by atmospheric air. Depending on the temperature of the experiment, different fluxes consisting of $ZnCl_2$ with the addition of other low-melting point salts (for example, eutectics of $ZnCl_2$ with NH_4Cl or KCl) are employed.

The surface of cobalt disc specimens, 11.28 ± 0.02 mm in diameter and 5–6 mm high, was ground flat and polished mechanically. Immediately before the experiment, the solid specimen was rinsed with ethanol and dried. Then, it was pressed into a graphite tube, 16 mm in diameter, to protect its lateral surface from interaction with the melt. Therefore, only the disc surface, 1 cm^2 area, dissolved in the liquid phase during the run. If a larger surface area was desirable to shorten the duration of experiments (for example, when determining the solubility values), while its instantaneous value was unimportant, the specimens with unprotected lateral surfaces were used. In such cases, graphite tubes served only as holders for cobalt specimens.

First, the flux was melted in a 26-mm inner diameter alumina crucible. The height of the flux column was around 15 mm. Pieces of a Sn-based alloy were then melted under the flux layer. The amount of the melt material taken was equivalent to a volume of the liquid phase of 10 cm^3 at a given temperature.

For preheating, the cobalt specimen rotating at the lowest available angular speed of 6.45 rad s^{-1} was lowered into the flux bulk, so that the distance between its surface and the top surface of the metallic melt column was around 10 mm. When the temperature had equilibrated (typically after 500 s), the specimen rotating at the required speed was lowered into the bulk of melt, so that the distance from the surface of the disc to the bottom of the crucible was 15.0 ± 0.5 mm. This was the start of the run. The rotating disc was held in the melt for a predetermined period of time. The run was then completed in one of two following ways.

(1)   When studying the dissolution process, the solid cobalt specimen was lifted from the melt into the middle of the flux column, and then the crucible—together with the melt, the flux, and the specimen—was rapidly cooled down in a water bath located below the electric furnace. After cooling down to room temperature, the melt material adhering to the surface of cobalt specimen was removed by melting in a muffle furnace and subsequent wiping. Then, the specimen was washed with water and alcohol, dried, and weighed. The accuracy of weighing was ± 0.00005 g. Because the specimen had also been weighed before the run, its mass loss during dissolution in the melt could be
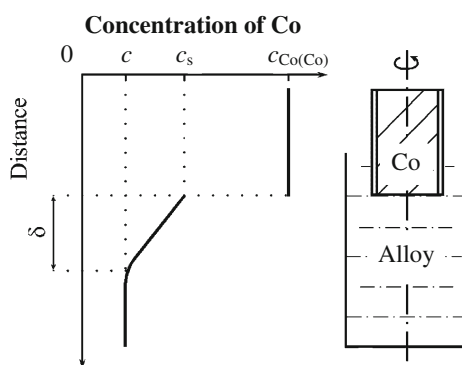
determined. Samples of the alloys obtained after the runs were analyzed chemically to determine their cobalt content (relative error not exceeded ±5%). Cobalt content was also found by electron probe microanalysis (EPMA) using a JEOL Superprobe-733 microanalyzer. Ten EPMA measurements were carried out on each Co–Sn–Bi–In–Zn–Sb sample, with the beam spot diameter being around 100 μm. The mean relative error of EPMA measurements was ±6%. The values of the cobalt content of the soldering alloys obtained by these three methods were then averaged and used in further calculations.

(2) When studying the growth kinetics of intermetallic-compound layers under conditions of their simultaneous dissolution in the liquid phase (with undersaturated melts), the crucible—together with the flux, the melt, and the solid specimen—was 'shot' into cold water with the help of a spring when the run ended to arrest the reactions at the interface of cobalt with the melt material. Note that the solid specimen continued to rotate until the solidification of the melt. The time of cooling the experimental cell from the experimental temperature down to room temperature did not exceed 2 s.

After cooling, the bimetallic specimen obtained was cut along the cylindrical axis using an electric-spark machine, ground flat, and polished electrolytically using the Elypovist apparatus. The cross sections prepared in such a way were examined metallographically with the help of MIM-7 microscope equipped with a HP Photosmart 720 camera. X-ray patterns were taken on DRON-3 and URS-50 apparatus using Cu K_α radiation. Electron probe microanalysis of the transition zone between cobalt and Sn-based alloys was also carried out. In this case, the beam spot diameter and the phase volume analyzed at each point were estimated to be about 1 μm and 2 μm^3, respectively.

To investigate the growth process of intermetallic-compound layers from the solder melts saturated with cobalt at a given temperature, experiments were carried out in a steel thermostat. The polished cobalt plates, 14 mm × 5 mm × 3 mm, were mounted onto the graphite crucibles, with an inner diameter of 11 mm and a height of approximately 16 mm. The crucibles were placed in the thermostat at a required temperature. These were then filled with the flux from a moveable electric-resistance furnace, kept at the same temperature. After the temperature in the thermostat had equilibrated, the crucibles were filled with the metallic melt, previously saturated with cobalt, from another moveable electric-resistance furnace also kept at the required temperature.

Cobalt was allowed to react with the melt during a predetermined period of time in the 300–1800 s range.

Then, the graphite crucibles with their contents were withdrawn from the thermostat and rapidly cooled down in water. Bimetallic specimens obtained were cut into two parts, normal to the long side of a cobalt plate. The cobalt–solder cross sections were prepared and examined as described above.

Results and discussion

Dissolution kinetics

The Nernst–Shchukarev equation is known to describe the dissolution process of a solid in a liquid phase under conditions of sufficiently intensive agitation (see, for example, [24, 37, 46, 47]). The differential form of this equation is

$$\frac{\mathrm{d}c}{\mathrm{d}t} = k\frac{s}{v}(c_\mathrm{s} - c), \tag{1}$$

where c is the instantaneous concentration of the dissolved substance in the bulk of the liquid phase, t is the time, c_s is the saturation concentration or solubility at a given temperature, k is the dissolution rate constant, s is the surface area of the solid in contact with the liquid, and v is the volume of the liquid phase. Integration with the initial condition $c = 0$ at $t = 0$ yields

$$c = c_\mathrm{s}\left[1 - \exp\left(-\frac{kst}{v}\right)\right] \tag{2}$$

or in another form

$$\ln\frac{c_\mathrm{s}}{c_\mathrm{s} - c} = k\frac{st}{v}. \tag{3}$$

Equations 1–3 indicate that the process of dissolution of a solid in a liquid is characterized by two quantities, namely, the solubility or saturation concentration, c_s, and the dissolution rate constant, k. If the pressure remains constant, the saturation concentration only depends on temperature. The dissolution rate constant is in addition dependent on the hydrodynamic conditions of flow of the liquid.

Solubility of cobalt in liquid soldering alloys

The solubility values may in principle be extracted from the liquidus curve of an appropriate binary phase diagram or from the isotherm on the isothermal section of a ternary phase diagram. Due to experimental difficulties, however, the position of these lines on many phase diagrams is rather uncertain. The Co–Sn binary system is no exception [38, 40–44]. Since for practical applications the solubility values must be known at a relative error not exceeding ±5%, the cobalt solubility in tin and the soldering alloys has been

determined experimentally by dissolving cylindrical cobalt specimens (2.75 cm^2 area) in the liquid phase until its saturation with cobalt atoms was attained.

From Eqs. 1–3, the concentration of any dissolved substance in the liquid phase is seen to increase with passing time and eventually to reach its limiting value, c_s, as was the case for the cobalt content in 87.5%Sn–7.5%Bi–3%In–1%Zn–1%Sb and 80%Sn–15%Bi–3%In–1%Zn–1%Sb soldering alloys (Fig. 2). These limiting values for tin and the alloys are listed in Table 1. Experimental values of c_s thus found are presented in the last column of this table.

As evidenced in Fig. 3, the temperature dependence of the solubility of cobalt in tin and the soldering alloys obeys a relation of the Arrhenius type:

$$c_s = A \exp(-E/RT), \tag{4}$$

where A is the frequency factor, E is the activation energy (enthalpy of dissolution), R is the gas constant, and T is the absolute temperature. The variation of $\ln c_s$ with $1/T$ is seen to be linear in all three cases. Application of the least-squares fit method yields the following equations:

$$c_s = 4.08 \times 10^2 \exp(-45200/RT)\% \text{ for Sn,}$$
$$c_s = 4.06 \times 10^2 \exp(-46300/RT)\% \text{ for an}$$
$$\quad 87.5\%\text{Sn}-7.5\%\text{Bi}-3\%\text{In}-1\%\text{Zn}-1\%\text{Sb alloy,}$$
$$c_s = 5.46 \times 10^2 \exp(-49200/RT)\% \text{ for an}$$
$$\quad 80\%\text{Sn}-15\%\text{Bi}-3\%\text{In}-1\%\text{Zn}-1\%\text{Sb alloy,}$$

where R is in J mol^{-1} K^{-1} (8.314 J mol^{-1} K^{-1}) and T in K. Appropriate linear regression coefficients are 0.9966, 0.9987, and 0.9963.

Comparison of the solubility values calculated from these three temperature dependences (smoothed solubilities)
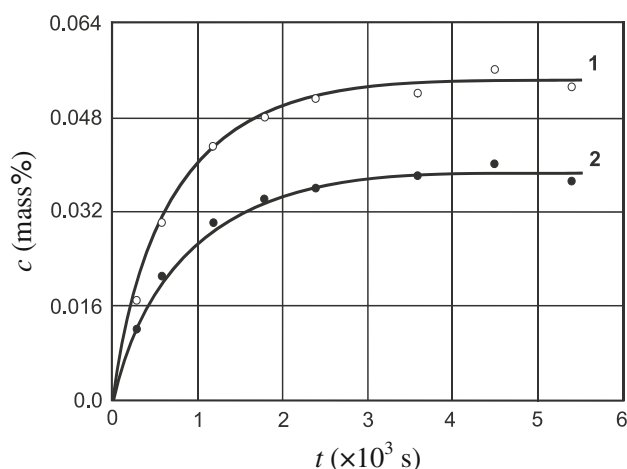

Fig. 2 Cobalt contents, dissolved into soldering alloys, are plotted against time to determine the solubility (saturation concentration), c_s. Temperature = 350 °C, rotational speed $\omega = 54.0$ rad s^{-1}, $s/v = 27.5$ m^{-1}. *1*, 87.5%Sn–7.5%Bi–3%In–1%Zn–1%Sb alloy; *2*, 80%Sn–15%Bi–3%In–1%Zn–1%Sb alloy

is provided in Table 2. The additives (Bi, In, Zn, and Sb) are seen to produce a considerable decrease of the cobalt solubility in the solder melts.

From the data of Table 2, it must be clear why conventional methods employed to investigate phase equilibria, for example differential scanning calorimetry, do not yield satisfactory results in the liquidus determination with systems like Co–Sn. First, the solubility values of cobalt in liquid tin are rather small. Second, the liquidus curve ascends very abruptly from the eutectic point to the peritectic temperature of formation of the CoSn$_2$ compound. For these reasons, any arrests on the thermal heating–cooling curves, corresponding to the cobalt solubility in tin (and the soldering alloys) at a given temperature, cannot be determined with confidence.

In contrast, the kinetic method employed here is sufficiently accurate because the degree of saturation of the liquid can easily be controlled by chemical and physical means. Since the experiment is carried out at constant temperature and pressure, no supersaturation of the liquid is possible. Sooner or later, an equilibrium intermetallic phase is formed at the cobalt–solder interface (see "Formation of intermetallic-compound layers"). At long dipping times, the layer of this (and perhaps some other) phase will grow until all the cobalt (the solder is taken in excess) is consumed completely. Note that for the liquid tin phase to reach saturation, it does not matter whether the saturation process is carried out from the cobalt phase, or from the nearest (to tin) intermetallic compound, or from any other intermetallic compound of the Co–Sn binary system because cobalt exists in the saturated metallic melt in the form of atoms, and therefore any initial phase decomposes during dissolution in tin. No compounds can occur within the liquid tin bulk unless the temperature is lowered enough to cause the supersaturation of the melt (pressure is usually constant in the course of experiments).

Dissolution rate constants and diffusion coefficients

Besides the solubility, c_s, another main characteristic of the dissolution process of a solid metal in a liquid solder is the dissolution rate constant, k. To obtain an accurate measure of this constant, the initials parts of the dissolution curves such as those shown in Fig. 3 were investigated in detail at an angular disc rotational speed of 24.0 rad s^{-1}. An example for a liquid 87.5%Sn–7.5%Bi–3%In–1%Zn–1%Sb alloy is shown in Fig. 4. The numerical values obtained are presented in Tables 3 and 4. The mean relative error of determination of the dissolution rate constant is ±8%. The linearity of a plot of $\ln[c_s/(c_s - c)]$ against st/v in Fig. 5 provides evidence for the validity of Eqs. 1–3 which can thus be used to determine accurate values of the dissolution rate constant.

Table 1 Experimental data on the determination of the cobalt solubility (saturation concentration), c_s, in tin and liquid soldering alloys

Alloy	Temperature (°C)	Time (s)	Cobalt content (%)			c_s (%)
			ML	EPMA	CA	
Sn	275	5400	0.018	0.024	0.020	0.020 ± 0.002
	300	5400	0.028	0.031	0.033	0.031 ± 0.003
	325	5400	0.048	0.043	0.045	0.045 ± 0.003
	350	5400	0.069	0.071	0.076	0.072 ± 0.004
	375	5400	0.094	0.084	0.084	0.087 ± 0.006
	400	5400	0.11	0.14	0.13	0.13 ± 0.02
	425	5400	0.16	0.14	0.19	0.16 ± 0.03
	450	5400	0.23	0.21	0.25	0.23 ± 0.03
87.5% Sn…	250	3600	0.0090	0.010	0.011	0.010 ± 0.001
		4500	0.0095	0.0097	0.010	
		5400	0.011	0.0092	0.0097	
	300	5400	0.023	0.025	0.024	0.024 ± 0.002
	350	3600	0.043	0.053	0.056	0.0053 ± 0.007
		4500	0.057	0.057	0.055	
		5400	0.047	0.059	0.052	
	400	5400	0.083	0.12	0.11	0.10 ± 0.02
	450	3600	0.19	0.21	0.14	0.19 ± 0.03
		4500	0.18	0.17	0.21	
		5400	0.19	0.16	0.22	
80% Sn…	250	3600	0.0078	0.0083	0.0071	0.0070 ± 0.0009
		4500	0.0059	0.0080	0.0055	
		5400	0.0058	0.0060	0.0084	
	300	5400	0.016	0.015	0.017	0.016 ± 0.002
	350	3600	0.033	0.039	0.042	0.038 ± 0.005
		4500	0.032	0.056	0.041	
		5400	0.034	0.034	0.033	
	400	5400	0.074	0.090	0.10	0.088 ± 0.009
	450	3600	0.17	0.16	0.15	0.15 ± 0.03
		4500	0.18	0.13	0.15	
		5400	0.15	0.16	0.15	

Rotational speed $\omega = 54.0$ rad s^{-1}, $s/v = 27.5$ m^{-1}

ML mass loss measurements, *EPMA* electron probe microanalysis, *CA* chemical analysis

Note that, although the solubility values of cobalt in the alloys at a given temperature differ considerably, appropriate dissolution rate constants are very close. This appears to be a general trend in the dissolution of transition metals and their alloys in liquid-metal melts. It means that, in spite of the great difference in solubility values, the rates, with which those are attained, are not so different. The former may differ by a few orders of magnitude, whereas the latter usually fall in the range (1–10) × 10^{-5} m s^{-1} at reasonable rates of agitation of the liquid [24, 37, 46, 47].

For a rotating disc, the dissolution rate constant, k, is related to the diffusion coefficient, D, of the solute atoms across the diffusion boundary layer at the solid–liquid interface into the bulk of the liquid, the melt viscosity, v, and the angular speed of rotation, ω, through the equation [48]

$$k = 0.62 D^{2/3} v^{-1/6} \omega^{1/2}. \tag{5}$$

From this equation, it follows that the k–$\omega^{1/2}$ dependence must be linear. To check it, the runs were carried at the disc rotational speeds of 6.45, 9.00, 15.3, 32.7, 54.0, and 82.4 rad s^{-1} in addition to those at 24.0 rad s^{-1}. The results are presented in Fig. 6 and Table 5. As seen in Fig. 6, the dependence of the dissolution rate constant on the square root of the disc rotational speed is indeed linear.
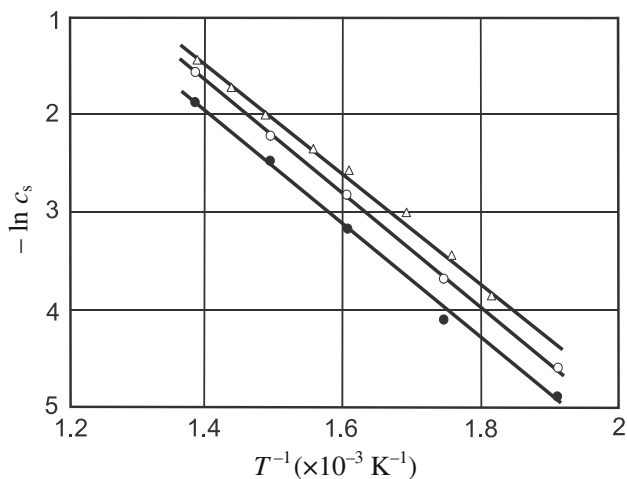
Fig. 3 Temperature dependence of the solubility of cobalt in tin and liquid soldering alloys. Δ—tin, ○—87.5%Sn–7.5%Bi–3%In–1%Zn–1%Sb alloy; ●—80%Sn–15%Bi–3%In–1%Zn–1%Sb alloy

Table 2 Comparison of smoothed cobalt solubility values in tin and soldering alloys at 250–450 °C

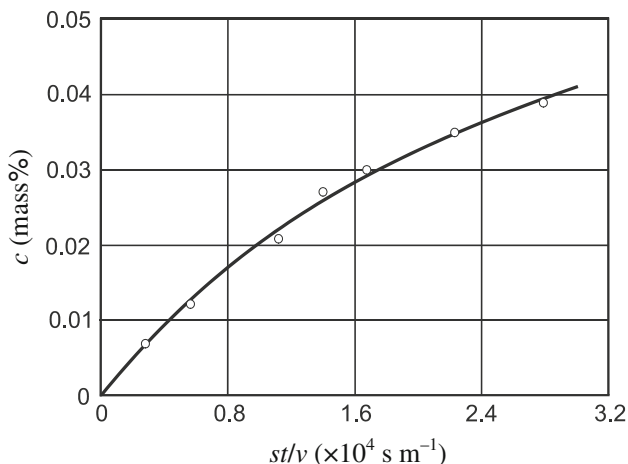| Temperature (°C)	Cobalt solubility, c_s (%)		
	Sn	87.5% Sn…	80% Sn…
250	0.012	0.0092	0.0067
300	0.031	0.024	0.018
350	0.066	0.053	0.041
400	0.13	0.10	0.083
450	0.22	0.18	0.15

Fig. 4 A plot of the concentration of cobalt, dissolved into a liquid 87.5%Sn–7.5%Bi–3%In–1%Zn–1%Sb alloy, against st/v. Temperature = 350 °C, rotational speed $\omega = 24.0$ rad s^{-1}, $s/v = 10.0$ m^{-1}

It provides evidence for a diffusion-controlled character of cobalt dissolution in liquid soldering alloys.

The diffusion coefficient, D, can clearly be determined from Eq. 5 if the dissolution rate constant is known, and

vice versa. It should be noted, however, that Eq. 5 is only valid for Schmidt's numbers, Sc, exceeding 1000.

The Schmidt number is a dimensionless parameter equal to the ratio of the kinematic viscosity to the diffusion coefficient: Sc = v/D. For liquid-metal melts, Sc is usually less than 1000. In such a case, a more accurate value of D can be obtained by using the equation [49]

$$k = 0.554 I^{-1} D^{2/3} v^{-1/6} \omega^{1/2}, \tag{6}$$

in which the factor I is a function of the Schmidt number: $I = f(\text{Sc})$. This equation is valid for Sc > 4. In the range $10 < \text{Sc} < 10^3$, typical of liquid metals, the difference in values of D determined using Eqs. 5 and 6 can be as high as 17% and as low as 3%.

To begin, an approximate value of the diffusion coefficient, D, was calculated according to Eq. 5 using known values of k, v [50], and ω. Next, the Schmidt number, Sc, and the correction factor, I, were found. Finally, the value of the diffusion coefficient was calculated from Eq. 6.

Following this procedure resulted in values of D presented in Table 6. The mean relative error of their determination is ±12%. Cobalt diffusion coefficients in liquid soldering alloys thus obtained are clearly averages for the concentration range 0–c_s. However, in view of the narrowness of this range, the concentration dependence of the diffusion coefficient may reasonably be expected to be insignificant.

Formation of intermetallic-compound layers

Two sets of experiments were carried out to visualize the effect of dissolution on the process of intermetallic-compound layer formation at the interface between cobalt and liquid soldering alloys. In the first set, the solder melt previously saturated with cobalt at a given temperature was employed. Therefore, dissolution of the solid cobalt specimens in the liquid phase did not occur. In the second, the melt initially contained no cobalt. Hence, the intermetallic layers were formed under conditions of their simultaneous dissolution in the solder melt, as illustrated schematically in Fig. 7. In this case, the cobalt disc was being rotated during the run at an angular speed of 24.0 rad s^{-1}.

Phase identity and chemical composition of intermetallic layers

A few backscattered electron images of the cobalt–solder transition zone are shown in Fig. 8 as an example. With both solders, a single-phase layer of the $CoSn_3$ intermetallic compound was found to form from both saturated and undersaturated melts at 250 °C and dipping times up to 1800 s. The layer of $CoSn_2$ occurred at 350 and 450 °C. Besides, the formation of an additional intermetallic layer

Table 3 Experimental results on the determination of the dissolution rate constant of cobalt in a liquid 87.5%Sn–7.5%Bi–3%In–1%Zn–1%Sb soldering alloy in the 250–450 °C temperature range

Temperature (°C)	Time (s)	Cobalt content (%)	$\ln[c_s/(c_s - c)]$	k ($\times 10^{-5}$ m s^{-1})
250	1500	0.0016	0.1911	1.3
	1800	0.0017	0.2043	1.1
	1800	0.0017	0.2043	1.1
	3000	0.0030	0.3947	1.3
300	1800	0.0096	0.5108	2.8
	3000	0.013	0.7802	2.6
350	300	0.0070	0.1417	4.7
	600	0.012	0.2567	4.3
	1200	0.021	0.5046	4.2
	1500	0.027	0.7122	4.7
	1800	0.030	0.8348	4.6
	2400	0.035	1.080	4.5
	3000	0.039	1.331	4.4
400	1200	0.047	0.6349	5.3
	1800	0.060	0.9163	5.1
450	300	0.030	0.1823	6.1
	600	0.054	0.3567	6.0
	1200	0.093	0.7270	6.1
	1500	0.11	0.9445	6.3
	1800	0.12	1.099	6.1
	2400	0.14	1.504	6.3

Rotational speed $\omega = 24.0$ rad s^{-1}, $s/v = 10.0$ m^{-1}

Table 4 Experimental results on the determination of the dissolution rate constant of cobalt in a liquid 80%Sn–15%Bi–3%In–1%Zn–1%Sb soldering alloy in the 250–450 °C temperature range

Temperature (°C)	Time (s)	Cobalt content (%)	$\ln[c_s/(c_s - c)]$	k ($\times 10^{-5}$ m s^{-1})
250	1200	0.0010	0.1616	1.3
	1800	0.0011	0.1793	1.0
	2400	0.0017	0.2927	1.2
	3000	0.0019	0.3335	1.1
	3600	0.0019	0.3335	0.9
300	1800	0.0069	0.4834	2.7
	3000	0.0092	0.7156	2.4
350	300	0.0051	0.1328	4.4
	600	0.010	0.2796	4.7
	1200	0.017	0.5355	4.5
	1500	0.019	0.6225	4.2
	1800	0.023	0.8232	4.6
	2400	0.026	1.006	4.2
	3000	0.030	1.316	4.4
400	1200	0.039	0.6347	5.3
	1800	0.050	0.9223	5.1
450	600	0.044	0.3471	5.8
	1500	0.092	0.9502	6.3
	2400	0.12	1.609	6.6

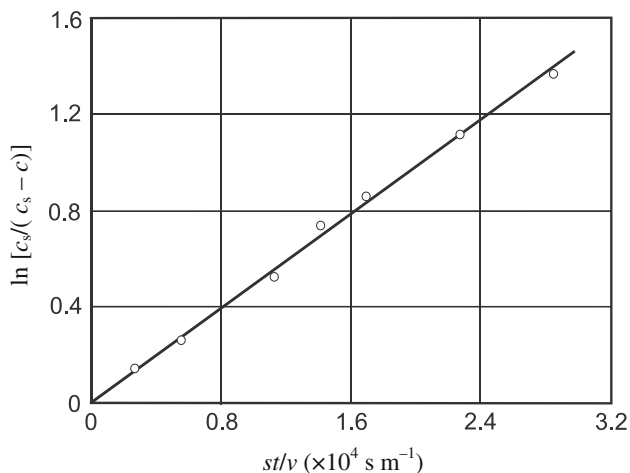Rotational speed $\omega = 24.0$ rad s^{-1}, $s/v = 10.0$ m^{-1}

Fig. 5 A plot of $\ln[c_s/(c_s - c)]$ against st/v for the data of Fig. 4
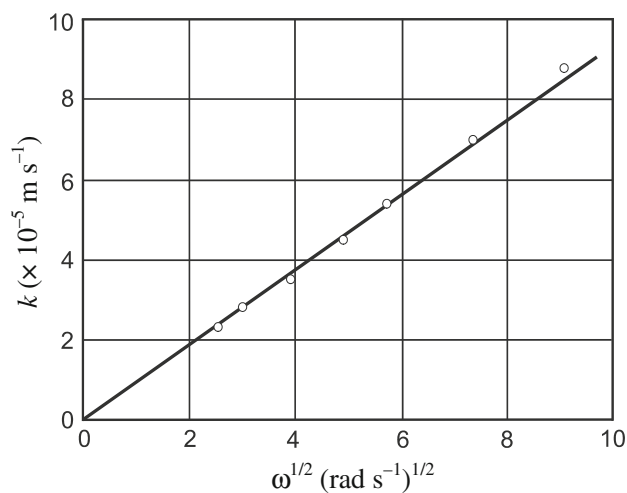

Fig. 6 A plot of the cobalt dissolution rate constant against the square root of the disc rotational speed for a liquid 87.5%Sn–7.5%Bi–3%In–1%Zn–1%Sb alloy. Temperature = 350 °C, s/v = 10.0 m^{-1}

around 1.5 μm thick was observed at 450 °C and a dipping time of 1800 s (Fig. 9).

Phase identification was carried out by X-ray diffraction (XRD). To prepare a specimen for X-ray examination, the melt material adhering to the solid cobalt base was removed by its rapid melting at an appropriate experimental temperature of 250, 350, or 450 °C. After slight polishing to remove the remainder of the melt material, cobalt specimens with adherent intermetallic layers proved suitable for X-ray analysis. Diffraction patterns were taken immediately from their surface.

At each temperature, similar patterns have been obtained with both soldering alloys investigated. To identify intermetallic phases formed at the interface between solid cobalt and liquid solders, comparison of our X-ray results with the literature data for the Co–Sn intermetallics

[51–60] was undertaken. Examples are shown in Figs. 10 and 11 and Tables 7 and 8.

As seen from Table 7, our experimental values of 2θ and interplanar distances (d-spacing) are in fair agreement with those reported for the α-CoSn$_3$ intermetallic compound having orthorhombic unit cell parameters $a = 1.6864$ nm, $b = 0.6268$ nm, and $c = 0.6270$ nm [51, 59]. However, two significant distinctions are worth noting.

First, our experimental peak intensities differ considerably from those reported in the literature (see Fig. 10; Table 7). It should be emphasized that the literature data themselves are somewhat confusing in this respect, giving quite different values of intensity for the same reflections. Most striking example is the intensity of the {312} reflection ($d = 0.2509$ nm). One database [58] reports $I = 1000$ for this reflection, whereas the other [59] indicates $I = 0$. This discrepancy is difficult to explain because both are based on the same work of Lang and Jeitschko [51].

Second, our experimental X-ray patterns for the α-CoSn$_3$ intermetallic compound contain a very broad, poorly resolved peak at about $2\theta = 14.1°$ ($d = 0.6278$ nm), missing from any pattern reported in the literature. If the intermetallic phases formed as separate layers growing between cobalt and solders at 250 °C are indeed the orthorhombic α-CoSn$_3$ compound, then this peak may originate from the {001} and {010} reflections.

It should be noted that earlier Chao et al. [60] also found the peak intensities to differ considerably from those reported for the equilibrium α-CoSn$_3$ intermetallic compound. Further X-ray work is needed to clarify the situation.

Literature XRD data for CoSn$_2$ are much more numerous than for CoSn$_3$ and agree very well with each other [52, 57, 59]. Good agreement is observed between those and our experimental X-ray results obtained at 350 and 450 °C (Fig. 11; Table 8). Hence, the constituent phase of intermetallic layers formed at the cobalt–solder interface at these temperatures is CoSn$_2$.

XRD data were confirmed by electron probe microanalysis (EPMA). As seen in Tables 9 and 10, the results of EPMA measurements are in accordance with the stoichiometry of the CoSn$_3$ and CoSn$_2$ intermetallic compounds. The distribution of cobalt and tin in the cobalt–solder transition zone is shown in Fig. 12. Both compounds appear to have a noticeable range of homogeneity. It is estimated as 25.5–22.5 at% (14.5–12.5%) Co for CoSn$_3$ at 250 °C (Table 11) and 34.6–31.1 at% (20.8–18.3%) Co for CoSn$_2$ at 450 °C (Table 12).

EPMA measurements showed a thin intermetallic layer formed between cobalt and CoSn$_2$ at 450 °C and a dipping time of 1800 s (see Fig. 9) to be CoSn. The average content of the components of this compound was found to be

Table 5 Experimental results on the determination of the dissolution rate constant of cobalt in liquid soldering alloys at different disc rotational speeds in the 6.45–82.4 rad s^{-1} range

Alloy	ω (rad s^{-1})	Time (s)	Co content (%)	$\ln[c_s/(c_s - c)]$	k ($\times 10^{-5}$ m s^{-1})
87.5% Sn…	6.45	3600	0.030	0.8348	2.3
	9.00	3000	0.030	0.8348	2.8
	15.3	2400	0.030	0.8348	3.5
	32.7	1800	0.033	0.9746	5.4
	54.0	1200	0.030	0.8348	7.0
	82.4	900	0.029	0.7922	8.8
80% Sn…	6.45	3600	0.023	0.8232	2.3
	9.00	3000	0.023	0.8232	2.7
	15.3	2400	0.024	0.8804	3.7
	32.7	1800	0.025	0.9410	5.2
	54.0	1200	0.023	0.8332	6.9
	82.4	900	0.022	0.7691	8.5

Temperature = 350 °C, s/v = 10.0 m^{-1}

Table 6 Evaluation of the diffusion coefficient of cobalt in liquid soldering alloys (ω = 24.0 rad s^{-1})

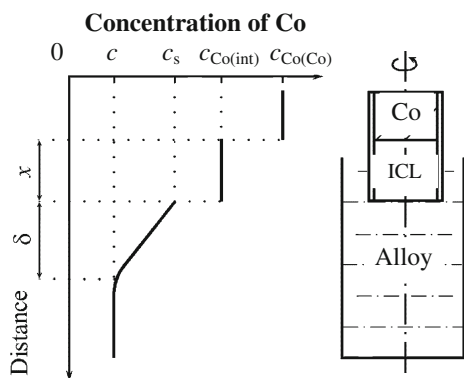| Alloy	Temperature (°C)	k ($\times 10^{-5}$ m s^{-1})	v ($\times 10^{-6}$ m^2 s^{-1}) [41]	D ($\times 10^{-9}$ m^2 s^{-1})	
				Eq. 5	Eq. 6
87.5% Sn…	250	1.2	0.24	0.17	0.19
	300	2.7	0.19	0.55	0.59
	350	4.5	0.18	1.17	1.28
	400	5.2	0.17	1.44	1.58
	450	6.2	0.15	1.82	2.02
80% Sn…	250	1.1	0.24	0.15	0.16
	300	2.4	0.19	0.46	0.49
	350	4.4	0.18	1.14	1.24
	400	5.2	0.17	1.44	1.58
	450	6.2	0.15	1.82	2.02

Fig. 7 Schematic diagram to illustrate the process of dissolution of solid cobalt in a liquid soldering alloy in the case where the intermetallic-compound layer (ICL = CoSn$_2$ or CoSn$_3$) is formed at the cobalt–solder interface. Not to scale. In fact, both the thickness, x, of the intermetallic layer and the thickness, δ, of the diffusion boundary layer at the solid–liquid interface is very small compared to the height of the liquid-alloy column

49.65 at% (32.85%) Co, 50.05 at% (66.69%) Sn, 0.06 at% (0.14%) Bi, 0.12 at% (0.16%) In, 0.12 at% (0.16%) Sb, and 0.00 at% (0.00%) Zn.

Our observations agree with the data on the phase equilibria in the Co–Sn system since according to Gao et al. [26], Cheng et al. [29], and Lang and Jeitschko [51] CoSn$_3$ decomposes peritectically at 345 °C and hence it cannot form a separate layer above this temperature. Probably, earlier investigators of the phase equilibria [38] have not revealed the CoSn$_3$ phase due to the very slow rate of the peritectic reaction of its formation [26, 29]. Sequential and not simultaneous occurrence of the CoSn$_2$ and CoSn layers in the temperature range of stability of these compounds is expected on the basis of kinetic considerations [37]. Note that, when studying the reaction kinetics of cobalt with pure tin, Zhu et al. [61] found the CoSn$_2$ layer to form at 400 and 500 °C, while the CoSn phase occurred at 600 °C.

Fig. 8 Backscattered electron images of the transition zone formed between cobalt and liquid soldering alloys at a dipping time of 1800 s. **a** Saturated melts. **b** Undersaturated melts ($\omega = 24.0$ rad s^{-1})
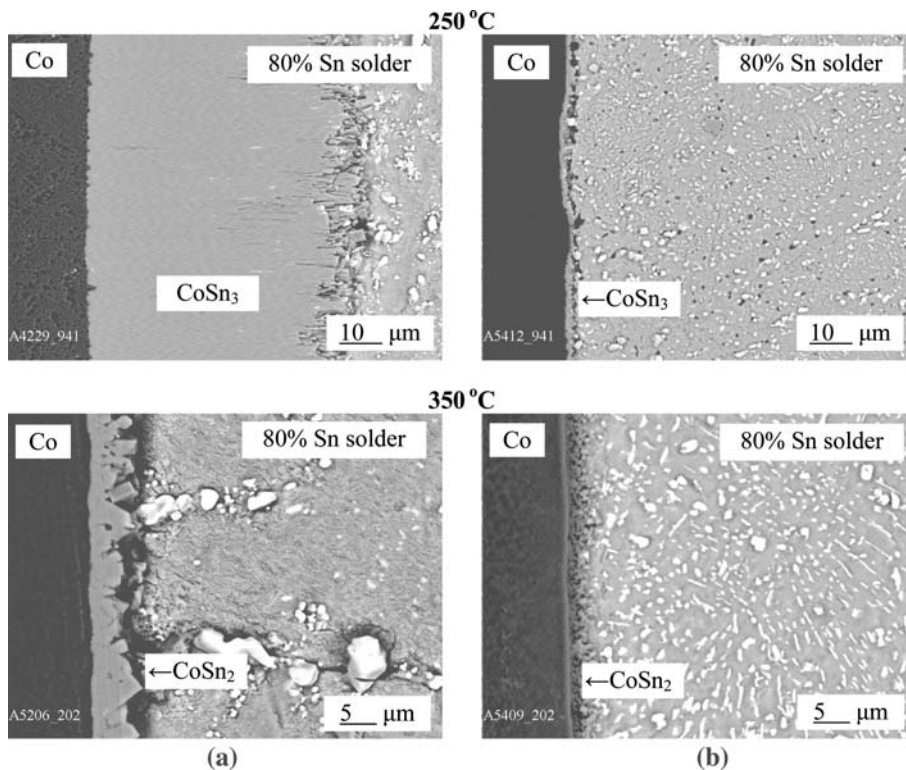

Fig. 9 Backscattered electron image and X-ray maps of intermetallic-compound layers formed between solid cobalt and liquid saturated soldering alloys at 450 °C and a dipping time of 1800 s
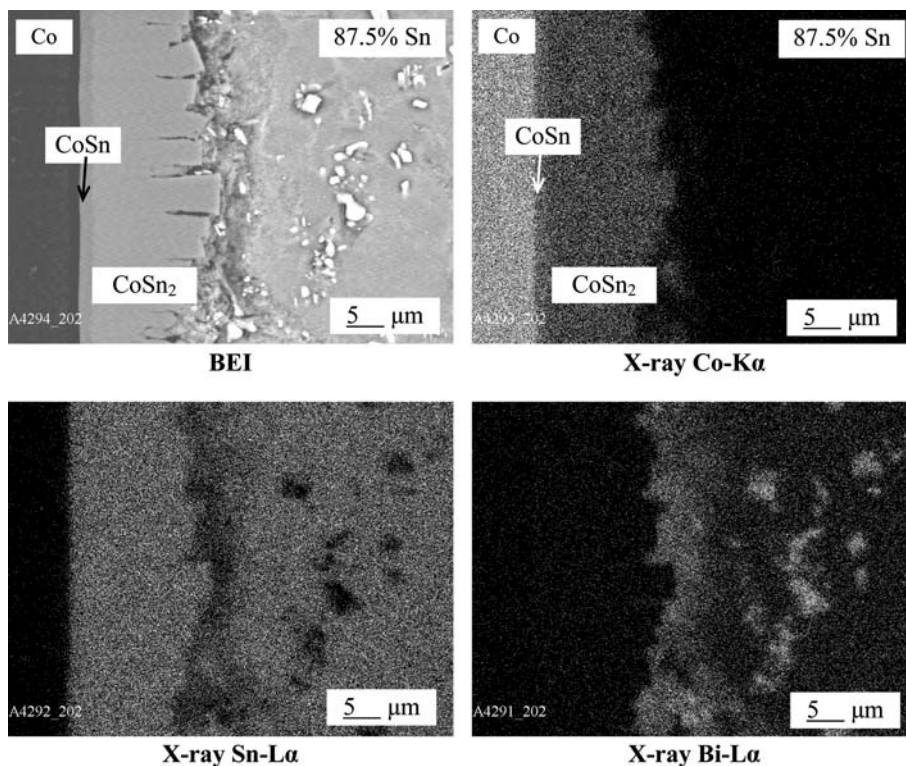
It is worth mentioning that, in addition to four intermetallic compounds Co$_3$Sn$_2$, CoSn, CoSn$_2$, and CoSn$_3$, formation of the CoSn$_4$ layer was observed by Wang and Chen at the corners of the Co–Sn diffusion couples reacted at 180–190 °C [62]. It is yet unclear whether the CoSn$_4$ phase is stable or metastable.

Fig. 10 Comparison of our experimental X-ray diffraction pattern (*top*) for an intermetallic phase formed at the interface between solid cobalt and a liquid cobalt-saturated 87.5%Sn–7.5%Bi–3%In–1%Zn–1%Sb soldering alloy at 250 °C and a dipping time of 1800 s with that (*bottom*) available in the literature for the α-CoSn₃ compound [51, 58, 59]. Cu K$_\alpha$ radiation
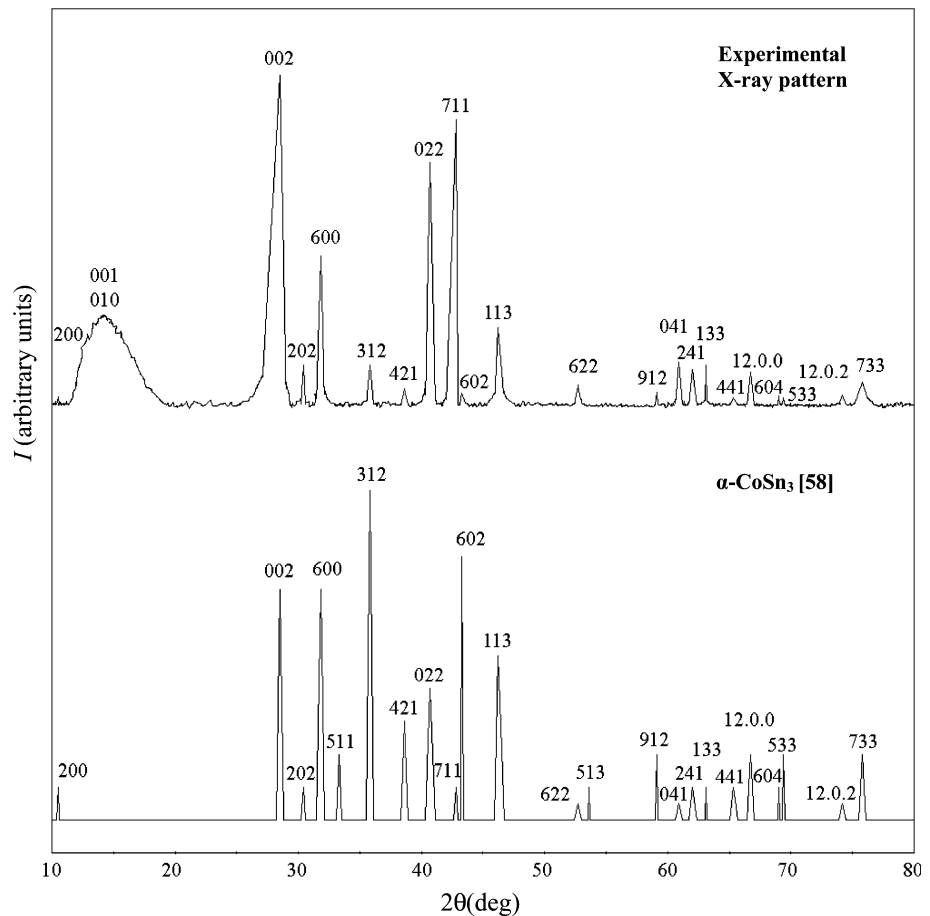
Most probably, occurrence of this phase is a result of the secondary reaction $Sn_{diff} + CoSn_3 = CoSn_4$ taking place at the $CoSn_3$–$CoSn_4$ interface where any contact between Co and $CoSn_3$ is lacking, i.e., actually in the $CoSn_3$–Sn diffusion couple. In the Co–$CoSn_3$–Sn couple, the $CoSn_4$ layer can hardly compete with the fast-growing $CoSn_3$ layer, and is therefore missing.

The absence of the $CoSn_4$ compound from the equilibrium phase diagram might be due to the difficulty of attaining the equilibrium state of Co–Sn alloys during their annealing at low temperatures. As evidenced from these data, further wok is required to establish phase equilibria in Sn-rich alloys of the Co–Sn binary system. Investigation of reaction kinetics in $CoSn_3$–Sn diffusion couples might be helpful in this respect because the reaction–diffusion process is known to be much more rapid than the conventional annealing of cast alloys (see [37]).

Mechanism of formation of intermetallic layers

Generally, growth of any intermetallic layer A_pB_q at the interface between a solid metal A and a liquid solder B saturated with A at a given temperature is a result of counter diffusion of components A and B across its bulk

followed by partial chemical reactions between diffusing atoms of one component and surface atoms of another component [37, 63]

$$qB_{diffusing} + pA_{surface} = A_pB_q \tag{7}$$

and

$$pA_{diffusing} + qB_{surface} = A_pB_q. \tag{8}$$

These reactions yield the increases, dx_{B1} and dx_{A2}, in layer thickness during a small period of time, dt, as shown in Fig. 13. The layer growth rate is

$$\left(\frac{dx}{dt}\right)_{growth} = \frac{k_{0B1}}{1 + \frac{k_{0B1}x}{k_{1B1}}} + \frac{k_{0A2}}{1 + \frac{k_{0A2}x}{k_{1A2}}} \tag{9}$$

where k_{0B1} and k_{0A2} are chemical constants, and k_{1B1} and k_{1A2} are diffusional constants (reaction–diffusion coefficients). With the saturated solder melt, the layer growth kinetics are thus initially linear (at x up to 500–600 nm) and then parabolic ($x > \sim 1$ μm) [37].

Effect of dissolution on the layer growth rate

As seen in Fig. 8, the thickness of intermetallic layers is much less in the case of the undersaturated solder melt

Fig. 11 Comparison of our experimental X-ray diffraction pattern (*top*) for an intermetallic phase formed at the interface between solid cobalt and a liquid cobalt-saturated 87.5%Sn–7.5%Bi–3%In–1%Zn–1%Sb soldering alloy at 450 °C and a dipping time of 1800 s with that (*bottom*) available in the literature for the $CoSn_2$ compound [55, 59]. Cu K_α radiation
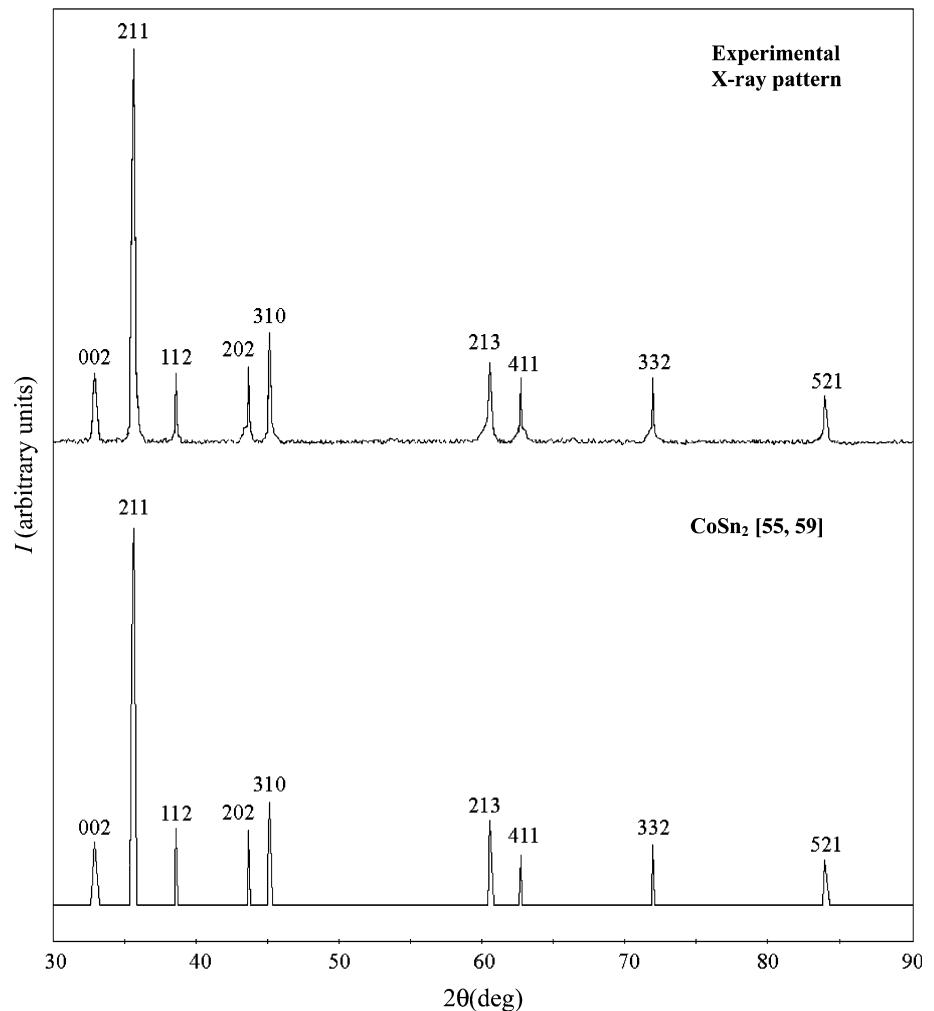
compared to the case of the saturated melt, other conditions being identical. Thus, the effect of dissolution on the layer growth kinetics at the cobalt–solder interface is very appreciable and cannot be neglected. Its magnitude can readily be evaluated on the basis of physicochemical considerations.

As evidenced in Fig. 13, in the case of the undersaturated solder melt, the net rate of layer formation is the difference between the sum of the rates of its growth at interfaces 1 and 2 and the rate of dissolution at interface 2. The dissolution rate is [37]

$$\left(\frac{dx}{dt}\right)_{dissolution} = b_t = b_0 \exp(-at) \tag{10}$$

where $b_0 = c_s k/\rho\varphi$, $a = ks/v$, ρ is the density of the A_pB_q compound, φ is the content of A in A_pB_q in mass fractions; other quantities are as before.

A mathematical equation describing the A_pB_q growth kinetics at the A–B interface under conditions of dissolution in the liquid phase is

$$\frac{dx}{dt} = \frac{k_{0B1}}{1 + \frac{k_{0B1}x}{k_{1B1}}} + \frac{k_{0A2}}{1 + \frac{k_{0A2}x}{k_{1A2}}} - b_0 \exp(-at) \tag{11}$$

It is clear that generally the layer growth is nonparabolic. Moreover, if

$$k_{0B1} + k_{0A2} < b_0 \tag{12}$$

the A_pB_q layer must be missing from the A–B couple. It means that the sum of the rates of chemical reactions at the interfaces (and also the rate of direct reaction between A and B) is less than the initial rate of dissolution.

Note that in this case the reason for the absence of the A_pB_q intermetallic layer from the initial couple is purely kinetic and not thermodynamic. Also, it is not connected with nucleating a new phase, as is often assumed, because even an already existing intermetallic layer artificially formed at the cobalt–solder interface will inevitably disappear in the course of reaction, if the dissolution rate is maintained constant and equal to b_0. The latter condition is satisfied, if the solid metal surface is continuously washed

Table 7 Comparison of the literature X-ray data for the CoSn₃ compound [58, 59] with our experimental results for an intermetallic phase formed at the interface between cobalt and a liquid Co-saturated 87.5%Sn–7.5%Bi–3%In–1%Zn–1%Sb soldering alloy at 250 °C and a dipping time of 1800 s (Cu K$_\alpha$ radiation)

h	k	l	2θ (°)		d (nm)		I		2θ (°)	d (nm)	I
			[58]	[59]	[58]	[59]	[58]	[59]			
2	0	0	10.46	10.49	0.8453	0.8432	100	1000	10.5	0.8426	24
–	–	–	–	–	–	–	–	–	14.1	0.6278	270
0	0	2	28.45	28.47	0.3135	0.3135	700	68	28.5	0.3132	1000
2	0	2	30.38	30.42	0.2940	0.2938	100	4	30.4	0.2940	120
6	0	0	31.81	31.84	0.2811	0.2811	700	293	31.8	0.2813	451
5	1	1	33.34	33.38	0.2659	0.2684	200	48	–	–	–
3	1	2	35.73	35.79	0.2511	0.2509	1000	0	35.8	0.2508	120
4	2	1	38.54	38.57	0.2333	0.2334	300	367	38.6	0.2332	48
0	2	2	40.67	40.71	0.2217	0.2216	400	155	40.7	0.2217	735
7	1	1	42.71	42.72	0.2116	0.2117	100	23	42.8	0.2114	865
6	0	2	43.17	43.23	0.2094	0.2093	800	263	43.3	0.2090	36
1	1	3	46.06	45.10	0.1969	0.1969	500	100	46.2	0.1965	235
6	2	2	52.57	52.58	0.1740	0.1740	50	5	52.7	0.1737	60
5	1	3	53.57	53.62	0.1709	0.1709	100	66	–	–	–
9	1	2	59.28	59.32	0.1558	0.1558	200	0	59.1	0.1563	39
0	4	1	60.88	60.94	0.1520	0.1520	50	2	60.9	0.1520	129
2	4	1	61.98	62.03	0.1496	0.1496	100	91	62.0	0.1497	108
1	3	3	63.10	63.16	0.1472	0.1472	100	4	63.1	0.1473	120
4	4	1	65.23	65.24	0.1429	0.1430	100	81	65.3	0.1427	21
12	0	0	66.48	66.54	0.1405	0.1405	200	84	66.7	0.1402	99
6	0	4	68.47	68.54	0.1369	0.1369	100	35	69.0	0.1361	28
5	3	3	69.36	69.44	0.1354	0.1353	200	3	69.4	0.1354	21
12	0	2	73.82	73.90	0.1283	0.1282	50	11	74.2	0.1278	30
7	3	3	75.47	–	0.1259	–	200	–	75.8	0.1255	69

with a fresh solder melt or both the ratio of the solid surface area to the melt volume, s/v, and the reaction time, t, are sufficiently small.

As seen from Eq. 10, the dissolution rate decreases exponentially from b_0 to b_t in the 0–t time range. Hence, when

$$k_{0B1} + k_{0A2} = b_t \tag{13}$$

the A_pB_q layer occurs at the A–B interface after some delay. At large t, $b_t \approx 0$, and the layer growth kinetics become close to parabolic.

Equation 11 cannot be solved precisely. However, its simpler forms can readily be employed in practice.

Evaluation of intermetallic layer thickness

If the A_pB_q layer grows under conditions of diffusion control ($k_{0B1} \gg k_{1B1}/x$, $k_{0A2} \gg k_{1A2}/x$) while the dissolution rate is constant and equal to b_t, Eq. 11 reduces to

$$\frac{dx}{dt} = \frac{k_1}{x} - b_t \tag{14}$$

where only one diffusional (parabolic) constant, k_1, is retained for simplicity. In such a case, the layer thickness tends, with passing time, to a limiting value

$$x_{max} = \frac{k_1}{b_t} \tag{15}$$

defined from the condition $k_1/x - b_t = 0$.

Equation 15 is suitable for estimating the thickness of any intermetallic layer growing under conditions of its simultaneous dissolution in the liquid phase. Calculations are carried out twice for each point, t, by putting in the denominator of Eq. 15 first equal to $(b_0 + b_t)/2$ and then b_t. Thus, two sets of the layer thickness are obtained. The first set gives the underestimated values, x_{under}. The second yields the overestimated ones, x_{over}. Clearly, experimental values, x_{exp}, should lie somewhere in between.

Table 8 Comparison of the literature X-ray data for the CoSn$_2$ compound [55] with our experimental data for intermetallic phases formed at the interface between cobalt and a liquid cobalt-saturated 87.5%Sn–7.5%Bi–3%In–1%Zn–1%Sb soldering alloy at 350 and 450 °C and a dipping time of 1800 s (Cu K$_\alpha$ radiation)

Literature data [55]						Our experimental data					
						350 °C			450 °C		
h	k	l	2θ (°)	d (nm)	I	2θ (°)	d (nm)	I	2θ (°)	d (nm)	I
0	0	2	32.85	0.27260	155	33.0	0.2717	125.0	32.9	0.2723	170
2	1	1	35.60	0.25221	1000	35.6	0.2522	1000.0	35.6	0.2522	1000
1	1	2	38.62	0.23313	191	38.7	0.2327	227.2	38.7	0.2327	168
2	0	2	43.63	0.20698	185	43.8	0.2067	170.0	43.8	0.2067	184
3	1	0	45.07	0.20115	257	45.1	0.2010	333.3	45.0	0.2014	271
2	1	3	60.45	0.15315	210	60.5	0.1530	212.0	60.5	0.1530	197
4	1	1	62.57	0.14845	123	62.6	0.1482	118.3	62.6	0.1484	159
3	3	2	71.86	0.13137	149	71.9	0.1313	145.9	71.8	0.1314	159
5	2	1	83.79	0.11544	111	83.8	0.1154	106.7	83.9	0.1155	113

Note: Since any X-ray pattern contains over 50 reflections, the data in the table are restricted to most intensive reflections ($I > 100$ relative to the {211} reflection whose intensity is adopted as 1000 [52–57])

Table 9 Average Co, Sn, Bi, In, Zn, and Sb contents of intermetallic phases, found by EPMA measurements on the surface of X-ray diffraction specimens (cobalt-saturated soldering alloys)

Alloy	Reaction conditions		Content (at%)						Phase
	Temperature (°C)	Dipping time (s)	Co	Sn	Bi	In	Zn	Sb	
87.5% Sn	250	600	25.36	74.25	0.13	0.25	0.00	0.00	CoSn$_3$
		1200	24.84	73.27	0.77	0.80	0.02	0.30	
		1800	25.47	74.06	0.15	0.29	0.02	0.00	
	350	600	33.59	65.98	0.22	0.21	0.00	0.00	CoSn$_2$
		1200	33.07	66.59	0.05	0.27	0.02	0.00	
		1800	33.93	65.71	0.11	0.25	0.00	0.00	
	450	600	33.44	65.23	0.85	0.43	0.06	0.00	CoSn$_2$
		1200	43.11	65.32	0.15	0.42	0.00	0.00	
		1800	32.92	66.71	0.16	0.19	0.01	0.01	
80% Sn	250	600	24.57	73.54	0.42	0.86	0.00	0.61	CoSn$_3$
		1200	24.91	74.16	0.23	0.48	0.00	0.22	
		1800	25.79	73.75	0.22	0.21	0.03	0.00	
	350	600	33.93	65.72	0.05	0.30	0.00	0.00	CoSn$_2$
		1200	32.96	66.54	0.10	0.39	0.00	0.00	
		1800	34.25	65.37	0.14	0.24	0.00	0.00	
	450	600	32.93	66.67	0.27	0.09	0.04	0.00	CoSn$_2$
		1200	33.99	65.03	0.31	0.36	0.31	0.00	
		1800	33.35	66.01	0.37	0.24	0.02	0.01	

When employing Eq. 15, the main difficulty to overcome is evaluating the diffusional growth-rate constant, k_1. It can be done as follows.

(1) If a single-phase intermetallic layer occurs in the case of both saturated and undersaturated melts, the value of k_1 is found from the experimental layer thickness–time dependence (parabolic relation) for the saturated melt. For example, in the case of the saturated 80%Sn–15%Bi–3%In–1%Zn–1%Sb alloy melt, the experimental value of the CoSn$_2$ layer thickness was found to be 33.0×10^{-6} m at

Table 10 Average Co, Sn, Bi, In, Zn, and Sb contents of intermetallic phases, found by EPMA measurements on metallographic cross sections

Alloy	Temperature (°C)	Content (at%)						Phase
		Co	Sn	Bi	In	Zn	Sb	
87.5% Sn	250	24.73	74.43	0.32	0.46	0.03	0.04	$CoSn_3$
	350	33.96	65.53	0.34	0.15	0.01	0.01	$CoSn_2$
	450	33.53	66.03	0.26	0.14	0.02	0.02	$CoSn_2$
80% Sn	250	25.18	73.56	0.56	0.59	0.05	0.06	$CoSn_3$
	350	32.94	66.39	0.19	0.25	0.02	0.01	$CoSn_2$
	450	33.57	65.99	0.25	0.16	0.01	0.02	$CoSn_2$

Six to ten measurements were made at random in the middle of intermetallic layers. Cobalt-saturated soldering alloys, dipping time = 1800 s

450 °C and a dipping time of 1800 s. Hence, $k_1 = x^2/2t = 3.0 \times 10^{-13}$ m^2 s^{-1}. Other quantities necessary for calculations are $k = 6.2 \times 10^{-5}$ m s^{-1} at $\omega = 24.0$ rad s^{-1}, $c_s = 10.74$ kg m^{-3} (0.15% Co in the soldering alloy), $\rho = 8.91 \times 10^3$ kg m^{-3} [56], $\varphi = 0.1989$ (19.89% Co in $CoSn_2$), $s/v = 10.0$ m^{-1}, and $b_0 = 3.76 \times 10^{-7}$ m s^{-1}.

Comparison of calculated values of the $CoSn_2$ layer thickness, x_{under} and x_{over}, with experimental ones, x_{exp}, is provided in Table 13. Since the duration of the soldering procedure rarely exceeds a few minutes, the agreement of these values appears to be quite sufficient for practical purposes to estimate the intermetallic-layer thickness at the solid–liquid interface.

(2) The layer growth-rate constant, k_1, is found from an experimental thickness–time dependence for the undersaturated melt using one or a few initial thickness values. Then, the other values can readily be calculated from Eq. 15, thereby reducing the amount of experimental work. For example, in the case of the undersaturated 87.5%Sn–7.5%Bi–3%In–1%Zn–1% Sb alloy melt at 350 °C, $k = 4.5 \times 10^{-5}$ m s^{-1} at $\omega = 24.0$ rad s^{-1}, $c_s = 3.75$ kg m^{-3} (0.053% Co in the soldering alloy), $b_0 = 9.52 \times 10^{-8}$ m s^{-1}, ρ_{int}, φ, and s/v are as before. The experimental value, x_{300}, of the $CoSn_2$ layer thickness at this temperature and dipping time of 300 s is 0.6×10^{-6} m. By assuming $x_{300} = x_{max}$, one obtains from Eq. 15 $k_1 = x_{max}(b_0 + b_{300})/2 = 5.4 \times 10^{-14}$ m^2 s^{-1}. Comparison of calculated and experimental values of the $CoSn_2$ layer thickness is provided in Table 14. Also included in the table are the results for an 80%Sn–15%Bi–3%In–1%Zn–1%Sb alloy, obtained using the following quantities: $k = 4.4 \times 10^{-5}$ m s^{-1} at $\omega = 24.0$ rad s^{-1}, $c_s = 2.96$ kg m^{-3} (0.041% Co in the soldering alloy), $b_0 = 7.35 \times 10^{-8}$ m s^{-1}, $x_{exp} = 0.5 \times 10^{-6}$ m at $t = 300$ s, and $k_1 = 3.5 \times 10^{-14}$ m^2 s^{-1}.

Again, the agreement is fairly good for both alloys. It is also worth noting that the range in which the intermetallic-layer thickness can vary is rather narrow, even though the time interval (300–1800 s) is relatively wide.

(3) If the data on the solid-state layer growth rate are available, a value of k_1 can be estimated by extrapolation from the temperature dependence. Clearly, the temperature must not differ considerably in both cases. An example is

Fig. 12 Microstructure of the transition zone between solid cobalt and liquid soldering alloys, and concentration profiles of cobalt and tin in (a) $CoSn_3$ and (b) $CoSn_2$ intermetallic layers. Cobalt-saturated solder melts, dipping time = 1800 s
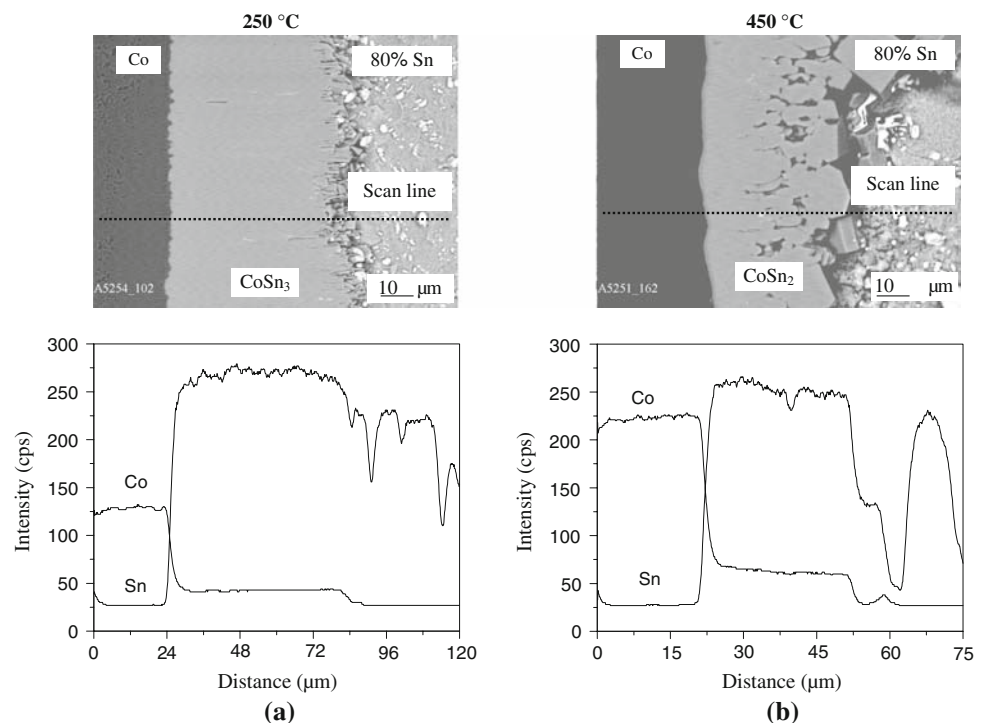
Table 11 Electron probe microanalysis data of the diffusion zone between cobalt and an 80%Sn–15%Bi–3%In–1%Zn–1%Sb soldering alloy

Phase	Place of measurement	Content (at.%)					
		Co	Sn	Bi	In	Zn	Sb
	At distance l away from the cobalt–intermetallic interface						
Co	$l = -100$ μm	100.00	0.00	0.00	0.00	0.00	0.00
	−50	100.00	0.00	0.00	0.00	0.00	0.00
	−25	99.94	0.06	0.00	0.00	0.00	0.00
	−15	100.00	0.00	0.00	0.00	0.00	0.00
	−10	100.00	0.00	0.00	0.00	0.00	0.00
	−5	99.96	0.04	0.00	0.00	0.00	0.00
CoSn$_3$	$l = 6$ μm	25.53	73.50	0.07	0.57	0.00	0.33
	12	24.71	73.60	0.09	0.53	0.04	1.03
	18	24.48	74.90	0.06	0.44	0.02	0.11
	24	24.04	74.11	0.65	0.46	0.04	0.69
	30	23.90	74.24	0.37	0.51	0.04	0.94
	36	23.21	75.03	0.33	0.31	0.06	1.07
	42	22.53	74.56	1.13	0.70	0.04	1.04
	48	22.42	75.25	0.49	0.73	0.05	1.06
	At distance l away from the intermetallic–solder interface						
Solder	$l = 10$ μm	0.18	93.69	3.49	1.31	0.30	1.03
	20	1.04	94.94	1.57	1.40	0.01	1.04
	30	1.71	95.58	10.49	1.02	0.35	0.85
	50	0.02	80.28	17.49	1.22	0.09	0.90
	75	0.71	93.26	3.58	1.00	0.51	0.94
	100	0.07	96.41	1.59	0.88	0.34	0.70

Temperature = 250 °C, dipping time = 1800 s

Note: From this table, the range of homogeneity of the CoSn$_3$ compound formed at the cobalt–solder interface at 250 °C is seen to be around 25.5–22.5 at% (14.5–12.5%) Co

Table 12 Electron probe microanalysis data of the diffusion zone between cobalt and an 80%Sn–15%Bi–3%In–1%Zn–1%Sb soldering alloy

Phase	Place of measurement	Content (at%)					
		Co	Sn	Bi	In	Zn	Sb
	At distance l away from the cobalt–intermetallic interface						
Co	$l = -100$ μm	99.91	0.06	0.02	0.00	0.00	0.01
	−50	99.87	0.08	0.02	0.01	0.00	0.02
	−25	99.89	0.11	0.00	0.00	0.00	0.00
	−15	99.85	0.14	0.00	0.00	0.01	0.00
	−10	99.76	0.19	0.03	0.01	0.02	0.00
	−5	99.58	0.34	0.06	0.01	0.01	0.00
CoSn$_2$	$l = 6$ μm	34.55	65.21	0.06	0.17	0.01	0.00
	12	33.83	66.00	0.02	0.14	0.00	0.01
	18	33.45	66.37	0.03	0.13	0.01	0.01
	24	33.06	66.73	0.05	0.16	0.00	0.00
	30	32.40	67.43	0.02	0.15	0.00	0.00
	36	31.08	68.72	0.06	0.11	0.02	0.01
	At distance l away from the intermetallic–solder interface						
Solder	$l = 10$ μm	1.46	93.44	1.44	0.69	0.00	2.97
	20	0.60	95.48	0.94	0.56	0.02	2.41
	30	0.35	94.91	1.05	0.43	0.02	3.24
	50	0.21	95.96	0.68	0.32	0.00	2.85
	75	0.32	96.10	2.31	0.35	0.31	0.91
	100	0.17	96.96	0.98	0.46	0.02	1.42

Temperature = 450 °C, dipping time = 1800 s

Note: From this table, the range of homogeneity of the CoSn$_2$ compound formed at the cobalt–solder interface at 450 °C is seen to be around 34.6–31.1 at% (20.8–18.3%) Co
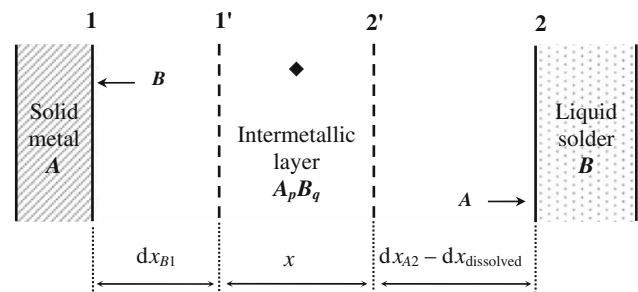
Fig. 13 Schematic diagram to illustrate the process of formation of the A_pB_q intermetallic layer under conditions of its simultaneous dissolution in the solder melt. Changes in layer thickness are measured relative to an inert marker (♦) located in its bulk

calculations of the NiBi$_3$ layer thickness at the interface between nickel and bismuth or Bi-base alloys [47].

Tensile strength of cobalt-to-solder joints

The cobalt-to-solder transition joints, 33–35 mm long, were made by means of interaction of solid cobalt specimens, 8 mm in diameter, with soldering alloy melts under strictly specified conditions of temperature, time, and liquid agitation, followed by their joint cooling at a controlled rate until the melt crystallizes. Their uniaxial tensile tests were carried out on a P-500 tester. The gage length of the Sn-alloy part was 8–12 mm, whereas the diameter was 5.9–7.8 mm. During the tensile tests, the crosshead speed was equal to 0.1 mm s^{-1}.

The failure occurred in a brittle manner (Fig. 14) with a slight plastic deformation either along or 2–5 mm away from the interface between dissimilar materials. The rupture strength, σ, was 95 ± 3 MPa with an 87.5%Sn–7.5%Bi–3%In–1%Zn–1%Sb soldering alloy and 104 ± 4 MPa with an 80%Sn–15%Bi–3%In–1%Zn–1%Sb soldering alloy. These values are more than two times greater than those (37–42 MPa [39]) for conventional Sn–Pb solders. The relative elongation was 2.0–2.6%.

Table 13 Calculated and experimental thicknesses of the $CoSn_2$ intermetallic layer grown from undersaturated 80%Sn–15%Bi–3%In–1%Zn–1%Sb solder melts at 450 °C ($\omega = 24.0$ rad s^{-1})

Time (s)	b_t ($\times 10^{-7}$ m s^{-1})	$(b_0 + b_t)/2$ ($\times 10^{-7}$ m s^{-1})	x_{under} ($\times 10^{-6}$ m)	x_{exp} ($\times 10^{-6}$ m)	x_{over} ($\times 10^{-6}$ m)
300	3.12	3.44	0.80	0.8 ± 0.1	0.87
600	2.59	3.18	0.94	1.0 ± 0.2	1.16
1200	1.79	3.02	1.00	1.5 ± 0.2	1.68
1800	1.23	2.50	1.20	1.8 ± 0.2	2.43

Table 14 Calculated and experimental thicknesses of the $CoSn_2$ intermetallic layer grown from undersaturated solder melts at 350 °C ($\omega = 24.0$ rad s^{-1})

Alloy	Time (s)	b_t ($\times 10^{-8}$ m s^{-1})	$(b_0 + b_t)/2$ ($\times 10^{-8}$ m s^{-1})	x_{under} ($\times 10^{-6}$ m)	x_{exp} ($\times 10^{-6}$ m)	x_{over} ($\times 10^{-6}$ m)
87.5% Sn	600	7.27	8.40	0.64	0.7 ± 0.1	0.74
	1200	5.55	7.54	0.72	0.8 ± 0.2	0.97
	1800	4.24	6.88	0.78	1.1 ± 0.3	1.27
80% Sn	300	6.44	6.90	0.54	0.6 ± 0.1	0.62
	600	5.64	6.50	0.60	0.8 ± 0.2	0.81
	1200	4.33	5.84	0.66	1.0 ± 0.3	1.05

Fig. 14 Transition joint of cobalt with a Co–87.5%Sn–7.5%Bi–3%In–1%Zn–1%Sb soldering alloy (**a**) before and (**b**) after tensile tests. *Arrow* indicates the place of rupture
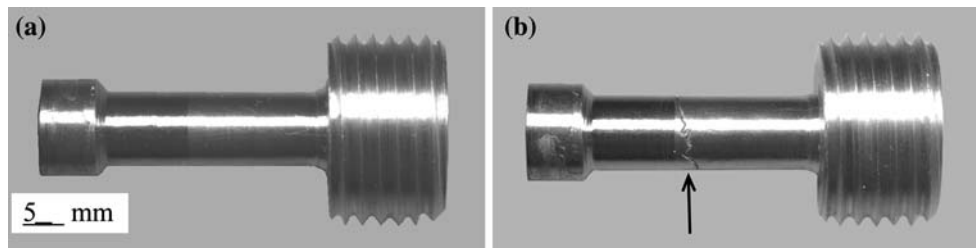
Figure 15 shows that even with specimens failing along the interface, the majority of the alloy grains remain adherent to the cobalt base. This means that metallurgical bonding between the joint constituents is rather strong.

Conclusions

The dissolution process of cobalt in liquid 87.5%Sn–7.5%Bi–3%In–1%Zn–1%Sb and 80%Sn–15%Bi–3%In–1%Zn–1%Sb soldering alloys is characterized by two quantities: the solubility, c_s, and the dissolution rate constant, k. The temperature dependence of the solubility of cobalt in those alloys is described in the 250–450 °C range by an equation of the Arrhenius type $c_s = A\exp(-E/RT)$, where $A = 4.06 \times 10^2\%$ and $E = 46.3$ kJ mol^{-1} for the former alloy and $A = 5.46 \times 10^2\%$ and $E = 49.2$ kJ mol^{-1} for the latter. Appropriate values for tin are $A = 4.08 \times 10^2\%$ and $E = 45.2$ kJ mol^{-1}.

The dissolution rate constants are rather close for these soldering alloys and vary in the range $(2–9) \times 10^{-5}$ m s^{-1} at disc rotational speeds of 6.45–82.4 rad s^{-1}.

With both alloys, the $CoSn_3$ intermetallic layer is formed at the interface of cobalt and the cobalt-saturated or undersaturated solder melt at 250 °C and dipping times up to 1800 s, whereas the $CoSn_2$ intermetallic layer occurs at higher temperatures of 350–450 °C. Formation of an additional intermetallic layer (around 1.5 μm thick) of the $CoSn$ phase was only observed at 450 °C and a dipping time of 1800 s.

A simple mathematical equation was proposed to evaluate the intermetallic-layer thickness in the case of undersaturated melts. Good agreement was observed between calculated and experimental values of layer thickness.

The tensile strength of the cobalt-to-solder joints was found to be 95 ± 3 MPa with an 87.5%Sn–7.5%Bi–3%In–1%Zn–1%Sb soldering alloy and 104 ± 4 MPa with an

Fig. 15 Secondary electron image of fracture surfaces of transition joints of cobalt with soldering alloys. **a** Cobalt part. **b** Alloy part

Co–87.5% Sn-7.5% Bi-3% In-1% Zn-1% Sb alloy

Co–80% Sn-15% Bi-3% In-1% Zn-1% Sb alloy

(a)　　　　　(b)
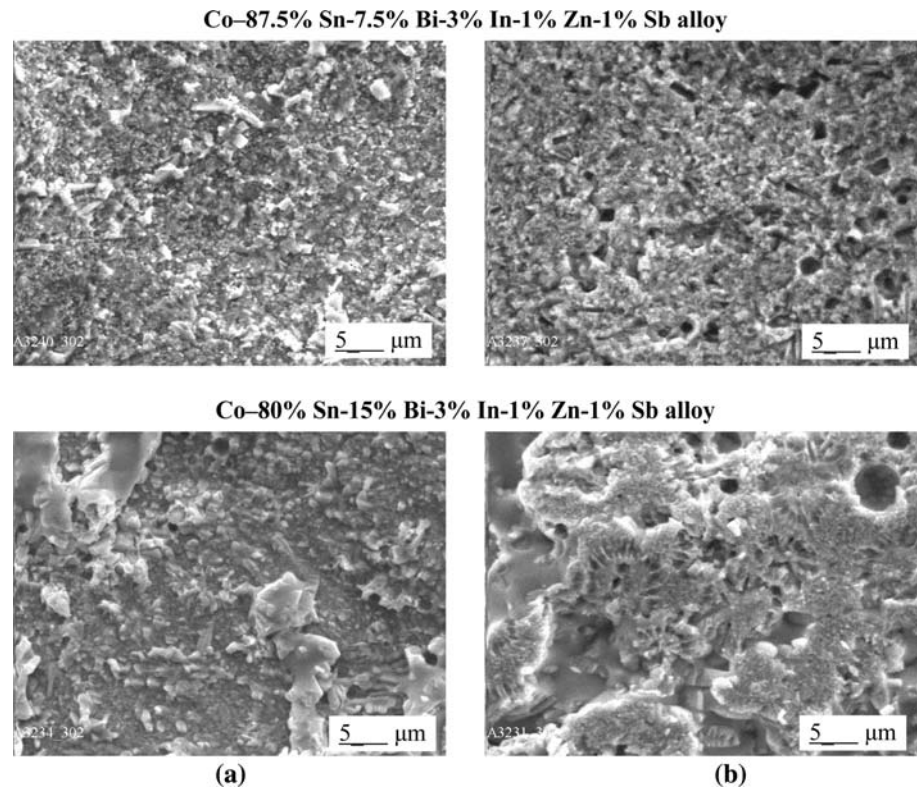
80%Sn–15%Bi–3%In–1%Zn–1%Sb soldering alloy. The plasticity of cast alloys is rather low, with the relative elongation being 2.0–2.6%.

References

1. Frear DR (1999) JOM 51:22
2. Lee MS, Chen C, Kao CR (1999) Chem Mater 11:292
3. Tao WH, Chen C, Ho CE, Chen WT, Kao CR (2001) Chem Mater 13:1051
4. Lalena JN, Dean NF, Weiser MW (2002) J Electron Mater 31:1244
5. Chiu MY, Wang SS, Chuang TH (2002) J Electron Mater 31:494
6. Alam MO, Chan YC, Tu KN (2003) J Appl Phys 94:4108
7. Yoon J-W, Kim S-W, Koo J-M, Kim D-G, Jung S-B (2004) J Electron Mater 33:1190
8. Lee H-T, Lin H-S, Lee C-S, Chen P-W (2005) Mater Sci Eng A 407:36
9. Liu PL, Shang JK (2005) Scripta Mater 53:631
10. Rizvi MJ, Chan YC, Bailey C, Lu H, Islam MN (2006) J Alloys Compd 407:208
11. Wang C-h, Chen S-w (2006) Acta Mater 54:247
12. Suganuma K, Lee J-E, Kim K-S (2007) In: Abstracts MRS 2007 Spring meeting, San Francisco, CA, 9–13 April 2007, E1.6
13. Bieler T, Borgesen P, Xing Y, Lehman L, Cotts E (2007) In: Abstracts of MRS 2007 Spring meeting, San Francisco, CA, 9–13 April 2007, E4.6
14. Chason E, Reinbold L, Jadhav N, Kelly V, Shin JW, Buchovecky E, Hariharaputran R, Kumar S (2007) In: Abstracts of MRS 2007 Spring meeting, San Francisco, CA, 9–13 April 2007, E2.4
15. Ursula K, Moon K, Handwerker C (2007) In: Abstracts of materials science and technology 2007 conference and exhibition, Detroit, MI, 16–20 September 2007, p 344
16. Anderson IE, Walleser J, Rehbein D, Kracher A, Harringa J (2007) In: Abstracts of materials science and technology 2007 conference and exhibition, Detroit, MI, 16–20 September 2007, p 344
17. Grossklaus KA, Handwerker CA, Stach EA, Revur RR, Sengupta S, Hwang H (2007) In: Abstracts of materials science and technology 2007 conference and exhibition, Detroit, MI, 16–20 September 2007, p 345
18. Ogunseitan OA (2007) JOM 59(7):12
19. Subramanian KN (ed) (2007) Lead-free electronic solders. Springer, Berlin, 378 pp
20. Tu KN (2007) Solder joint technology. Springer, Berlin, p 370
21. Zhu W, Wang J, Liu H, Jin Z, Gong W (2007) Mater Sci Eng 456:109
22. Wang H, Wang F, Gao F, Ma X, Qian Y (2007) J Alloys Compd 433:302
23. Lin C-T, Hsi C-S, Wang M-C, Chang T-C, Liang M-K (2008) J Alloys Compd 459:225
24. Barmak K, Berry DC, Khoruzha VG, Sidorko VR, Meleshevich KA, Samelyuk AV, Dybkov VI (2008) In: Proceedings of the materials science and technology conference: Pb-free, Pb-bearing joining and packaging materials and processes for microelectronics, Pittsburgh, PA, 5–9 October 2008, p 262
25. Cheng F, Nishikawa H, Takemoto T (2008) J Mater Sci 43:3643. doi:10.1007/s10853-008-2580-7

26. Gao F, Cheng F, Nishikawa H, Takemoto T (2008) Mater Lett 62:2257
27. Liu CZ, Zhang W (2009) J Mater Sci 44:149. doi:10.1007/s10953-008-3118-8
28. Ma H, Suhling JC (2009) J Mater Sci 44:1141. doi:10.1007/s10853-008-3125-9
29. Cheng F, Gao F, Nishikawa H, Takemoto T (2009) J Alloys Compd 472:530
30. Wang F, O'Keefe M, Brinkmeyer B (2009) J Alloys Compd 477:267
31. Wang YW, Chang CC, Kao CR (2009) J Alloys Compd 478:L1
32. Wang YW, Lin YW, Tu CT, Kao CR (2009) J Alloys Compd 478:121
33. Hauffe K (1955) Reaktionen in und an festen Stoffen. Springer, Berlin
34. Seith W (1955) Diffusion in metallen. Springer, Berlin
35. Hedvall JA (1966) Solid state chemistry. Elsevier, Amsterdam
36. Chebotin VN (1982) Fizicheskaya khimiya tverdogo tela. Khimiya, Moskwa
37. Dybkov VI (2002) Reaction diffusion and solid state chemical kinetics. IPMS, Kyiv
38. Hansen M (1958) Constitution of binary alloys. McGraw-Hill, New York
39. Lashko SV, Lashko NF (1988) Paika metallov. Mashinostroenie, Moskwa
40. Shunk FA (1969) Constitution of binary alloys: second supplement. McGraw-Hill, New York
41. Massalski TB, Murray JL, Bennett LH, Baker H (eds) (1986) Binary alloy phase diagrams, vol 2. American Society of Metals, Metals Park
42. Lyakishev NP (ed) (1999) Diagrammy sostoyaniya dvoynikh metallicheskikh sistem, vol 3, Part 1. Mashinostroenie, Moskwa
43. Jiang M, Sato J, Ohnuma I, Kainuma R, Ishida K (2004) Calphad 28:213
44. Okamoto H (2006) J Phase Equilib Diffus 27:308
45. Gurov KP, Kartashkin BA, Ugaste YuE (1981) Vzaimnaya diffusiya v mnogofaznikh metallicheskikh sistemakh. Nauka, Moskwa
46. Barmak K, Dybkov VI (2003) J Mater Sci 38:3249. doi:10.1023/A:1025129803413
47. Dybkov VI, Barmak K, Lengauer W, Gas P (2005) J Alloys Compd 389:61
48. Levich VG (1959) Fiziko-Khimicheskaya Hidrodinamika. Fizmatgiz, Moskwa
49. Kassner TF (1967) J Electrochem Soc 114:689
50. Vol AE (1962) Stroeniye i svoistva dvoynikh metallicheskikh system, vol 2. Fizmatgiz, Moskwa
51. Lang A, Jeitschko W (1996) Z Metallkd 87:759
52. Nial O (1938) Z Anorg Allg Chem 238:287
53. Matveyeva NM, Nikitina SV, Zezin SB (1968) Izv Akad Nauk SSSR Met 5:194
54. Djega Mariadassou C, Lecocq P, Michel A (1969) Ann Chim 4:175
55. Panteleimonov LA, Portnova GF, Nesterova OP (1971) Vestnik Moskov Univ Khimiya 26:79
56. Havinga EE, Damsma H, Hokkeling P (1972) J Less-Common Met 27:169
57. Buschow KHJ, van Engen PG, Jongebreur R (1983) J Magn Magn Mater 38:1
58. Cobalt Tin, ICDD, PDF2, 1999, File 00-02-0559, α-CoSn$_3$
59. Cobalt Tin, Pauling File Binary Edition, Inorganic Materials, 2002. http://crystdb.nims.go.jp
60. Chao Y-H, Chen S-W, Chang C-H, Chen C-C (2008) Metall Mater Trans A 39:477
61. Zhu W, Liu H, Wang J, Jin Z (2008) J Alloys Compd 456:113
62. Wang C-h, Chen S-w (2007) J Mater Res 22:3404
63. Dybkov VI (2009) JOM 61:78